Tellus (1981), *33*, 387–396

On the computational noise of finite-difference schemes used in ocean models

By MARY L. BATTEEN[1] and Y.-J. HAN, *Climatic Research Institute* and *Department of Atmospheric Sciences, Oregon State University, Corvallis, Oregon 97331, U.S.A.*

(Manuscript received June 18; in final form November 7, 1980)

ABSTRACT

As a guide for the choice of finite-difference schemes for use in ocean modeling, different distributions of variables over the horizontal array of grid points in an ocean circulation model are investigated using the shallow water equations. Numerical and analytical techniques are used to study the types of computational noise present in each grid system. It is shown that the B-scheme (in which the horizontal velocity is carried at the center and the height field is carried at each corner of a rectangular grid) with diffusive dissipation successively suppresses numerical noise in a coarse grid (>100 km) ocean model. For fine-scale resolution (<50 km), as in mesoscale ocean eddy models, it is shown that the C-scheme (in which the zonal velocity is carried at points to the east and west of the point of a rectangular grid where the height is carried, with the meridional velocity carried to the north and south of the height point) can be free of noise for the gravest mode (as in a two-layer model).

1. Introduction

Geostrophic motions in both the atmosphere and the ocean are possible because of geostrophic adjustment in which the dispersive property of the inertia-gravity waves is essential for restoring geostrophic balance whenever a local imbalance occurs (Rossby, 1938; Cahn, 1945; Mihaljan, 1963; Blumen, 1972). Clearly when numerical models are used for the simulation of geostrophic motions, the finite-difference schemes must be properly designed so that the dispersive properties of the inertia-gravity waves can be reasonably preserved in the models.

Studies by Winninghoff (1968), Arakawa and Lamb (1977) and Schoenstadt (1978) have examined the effect of different finite-difference schemes on the dispersive characteristics of inertia-gravity waves. These studies have shown that the simulation of the geostrophic adjustment process is highly dependent on both the choice of grid scheme (i.e., of the allocation of the pressure and horizontal velocity components over the points of a horizontal grid domain) and the ratio of the horizontal grid size to the Rossby radius of deformation, defined as the scale distance over which the gravitational tendency to render the free surface flat is balanced by the tendency of the Coriolis acceleration to deform the surface (Pedlosky, 1979). Arakawa and Lamb (1977), in particular, have recommended for atmospheric general circulation models (AGCMs) the use of the C-scheme (in which the zonal velocity is carried at points to the east and west of the point of a rectangular grid where the height is carried, with the meridional velocity carried to the north and south of the height point), since this scheme simulated geostrophic adjustment accurately when the grid size is smaller than the Rossby radius of deformation (~1000 km in the atmosphere). In global ocean general circulation models (OGCMs), however, horizontal grid sizes (>100 km), for practical reasons, are usually larger than the Rossby radius of deformation (~50 to 100 km for the first baroclinic mode in the ocean) and the choice of grid scheme in this case is not obvious.

[1] Present affiliation: The National Center for Atmospheric Research, P.O. Box 3000, Boulder, Colorado 80307, U.S.A.

0040-2826/81/040387-10$02.50/0 © 1981 Munksgaard, Copenhagen

The purpose of this study is to further examine the effect of different grid schemes on the geostrophic adjustment process with ocean modeling in mind. Since the shallow water equations govern the simplest fluid in which geostrophic adjustment can take place, we have utilized these equations for our study. The initial schemes considered are the A-, B-, C- and E-schemes, using Arakawa's (1972) nomenclature. However, detailed numerical tests are made only for the B- and C-schemes, since they are the only grid schemes currently in use in OGCMs (Bryan, 1969; Haney, 1974; Holland and Lin, 1975; Kim, 1979).

2. Finite-difference schemes and their frequency equations

The simplest fluid system in which geostrophic adjustment can take place is the two-dimensional, divergent, horizontal motion of an inviscid, incompressible fluid with a flat bottom and a free surface. The linearized shallow water equations in a Cartesian coordinate system which govern such motions are:

$$\partial u/\partial t - fv + g\partial h/\partial x = 0 \qquad (1)$$

$$\partial v/\partial t + fu + g\partial h/\partial y = 0 \qquad (2)$$

$$\partial h/\partial t + H(\partial u/\partial x + \partial v/\partial y) = 0 \qquad (3)$$

where u is the zonal velocity, v is the meridional velocity, h is the height of the free surface, f is the Coriolis parameter (assumed constant), H is the mean depth of the fluid, and g is gravity.

The different distributions of the dependent variables for the A-, B-, C- and E-grids, along with the finite-difference versions of eqs. (1)–(3) which were used, can be found in Mesinger and Arakawa (1976) or Arakawa and Lamb (1977). The distributions of the dependent variables h, u, and v on a rectangular grid for these schemes are reproduced in Fig. 1 for the reader's convenience. For schemes A, B and C, d is the grid size; in scheme E, $d^* = \sqrt{2}$ times d (which makes scheme E have the same number of points per unit area as any other scheme).

It should be noted that all of the schemes considered in the following analysis are semi-discrete, i.e., only space-differencing is used, so that the effect of space- rather than time- finite-difference schemes on the behavior of inertia-gravity waves can be examined. Due to the particular allocation of variables in each grid scheme, some spatial averaging is required in order to compute either the components of the pressure gradient or Coriolis force except in the E-scheme. Averaging is introduced in the pressure gradient force for both the A- and B-schemes and in the Coriolis force for the C-scheme. As shown in previous studies (Arakawa, 1972; Arakawa and Lamb, 1977; Schoenstadt, 1978), the use of spatial averaging can result in distortions of the exact dispersion relations and introduce computational noise.

To analyze the distortions of inertia-gravity wave frequency associated with each grid scheme, the frequency relations were derived for the linear differential eqs. (1)–(3) and for each of the grids considered. The results for a plane wave of the form $\exp(i(kx + ly - \omega t))$ are:

Exact frequency equation:

$$\left(\frac{\omega}{f}\right)^2 = \lambda^2(k^2 + l^2) + 1 \qquad (4)$$

Scheme A:

$$\left(\frac{\omega}{f}\right)^2 = \left(\frac{\lambda}{d}\right)^2 [\sin^2 kd + \sin^2 ld] + 1 \qquad (5)$$

Scheme B:

$$\left(\frac{\omega}{f}\right)^2 = 4\left(\frac{\lambda}{d}\right)^2 [(\sin^2 \tfrac{1}{2}kd \cos^2 \tfrac{1}{2}ld) + (\cos^2 \tfrac{1}{2}kd \sin^2 \tfrac{1}{2}ld)] + 1 \qquad (6)$$

Scheme C:

$$\left(\frac{\omega}{f}\right)^2 = 4\left(\frac{\lambda}{d}\right)^2 [(\sin^2 \tfrac{1}{2}kd + \sin^2 \tfrac{1}{2}ld)] + \cos^2 \tfrac{1}{2}kd \cos^2 \tfrac{1}{2}ld \qquad (7)$$

Scheme E:

$$\left(\frac{\omega}{f}\right)^2 = \left(\frac{\lambda}{d^*}\right)^2 [\sin^2 kd^* + \sin^2 ld^*] + 1 \qquad (8)$$

Here ω is the frequency, λ the Rossby radius of deformation $\equiv (gH)^{1/2} f^{-1}$, k the zonal wave number and l the meridional wave number.

A comparison between the exact frequency eq. (4) and finite-difference analogues (5)–(8) shows the manner in which the finite-difference schemes distort the exact frequency equation. When the first

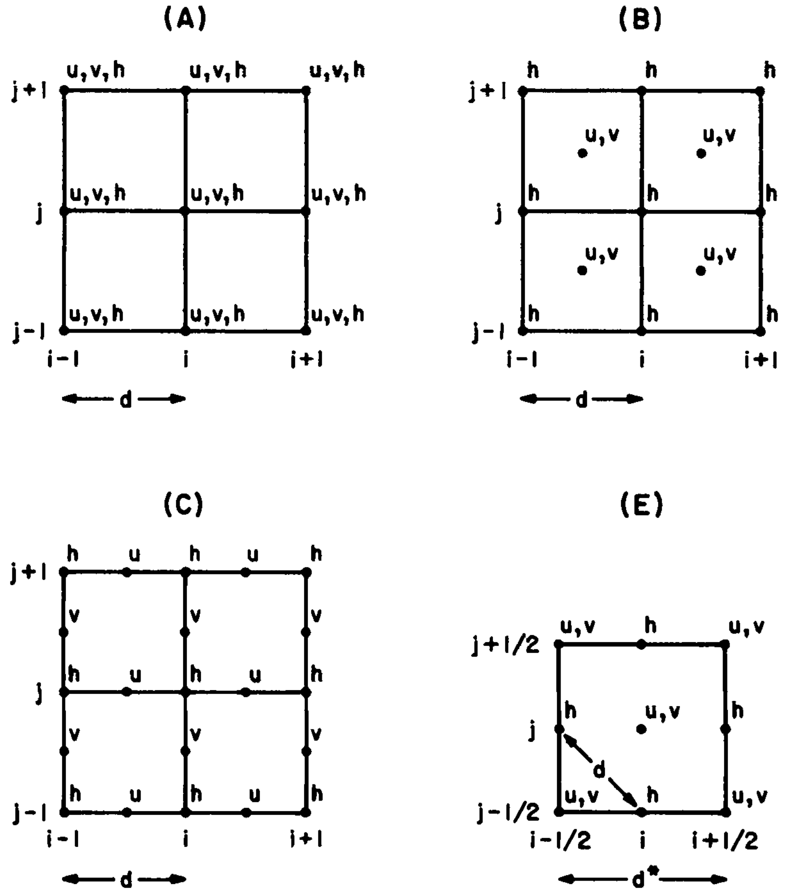

Fig. 1. Spatial distributions of the dependent variables on a rectangular grid. Here h is height, u and v are the eastward and northward velocity components, respectively, d is the grid size, $d^* = \sqrt{2}$ times d, and i and j are the indices of the grid points in the x and y directions respectively.

terms of each numerical scheme (i.e., those involving λ) are compared with the first term of the exact frequency equation, it is seen that whereas the non-dimensional frequency (ω/f) depends only on the parameters k, l, and λ in the continuous equation, the frequency (ω/f) depends also on the grid size d in all the finite-difference equations. Furthermore, the last term of each frequency equation (4)–(8) is unity except in the C-scheme (7).

The choice of grid size d will therefore influence the behavior of ω as a function of k and l, while the ratio of the Rossby radius of deformation to the grid size (λ/d) will determine whether the first or second term will dominate in the frequency equations: if the ratio is small, the second term will dominate, whereas if the ratio is large, the first term will dominate.

To illustrate this dependence, plots of the frequency (ω/f) obtained from the exact frequency equation and from the B-, C-, and E-grids are shown in Fig. 2 for $\lambda/d = 2$ and in Fig. 3 for $\lambda/d = 1/4$. The plot for the A-grid is not shown, since the frequency equation for this scheme is the same as that for the E-scheme. Since the Rossby radius of deformation for the first baroclinic mode in the ocean is of the order of 100 km, the (λ/d) ratios of 2 and 1/4 used in Figs. 2 and 3 correspond to grid sizes of 50 km and 400 km, respectively.

For $\lambda/d = 2$ (which was examined by Arakawa and Lamb, 1977), the frequency for the exact solution increases monotonically with wavenumber. The frequencies for both the B- and E-schemes agree with the frequency for the exact solution only in the third quadrant of the wave-

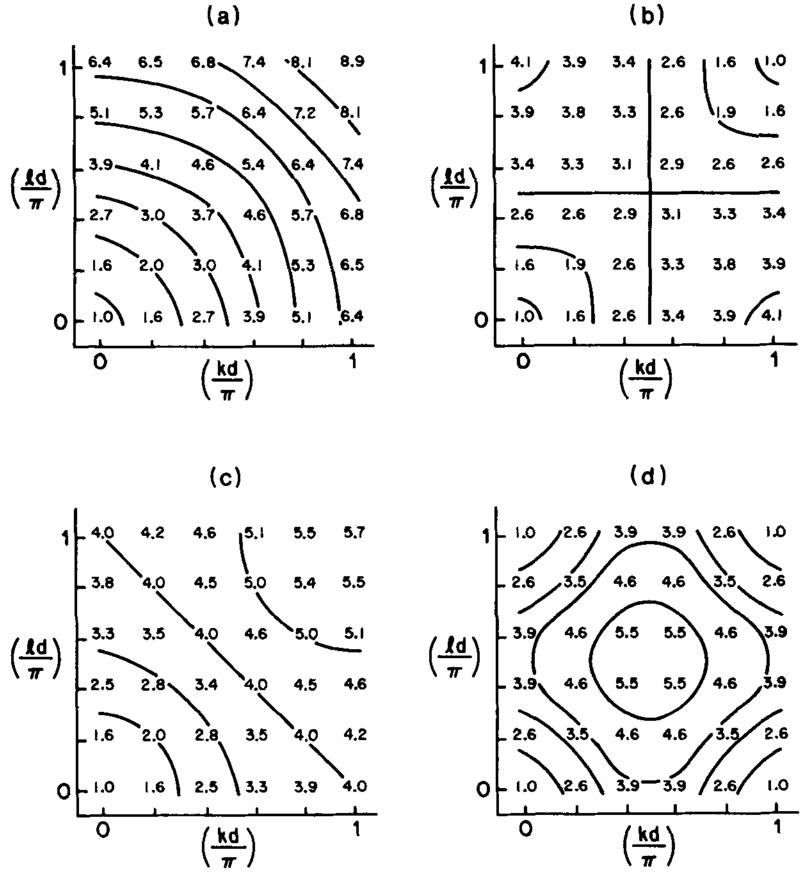

Fig. 2. Graphs of variation of (ω/f) as a function of the dimensionless wavenumbers for the exact frequency equation (a), the B-scheme (b), the C-scheme (c), and the E-scheme (d) for the case $\lambda/d = 2$. Here and in later figures $H = 4$ km, $f = 10^{-4}$ s^{-1}, and $g = 9.80$ m s^{-2}.

number domain; in the first quadrant, unlike the exact solution, the frequency decreases with increasing wavenumber. As a result, the propagation of two-dimensional short waves for these schemes is much slower than that for the exact solution. Furthermore, both schemes show an artificial frequency maximum at the mid-point resulting in zero group velocity and a consequent lack of energy propagation for this wavenumber. Unlike the other schemes, the C-scheme shows the same monotonic increase of frequency with increasing wavenumber as the exact solution so that proper simulation of the whole spectrum of waves occurs. Hence, an examination of the plots of each grid scheme show that the C-scheme best simulates the exact solution for $\lambda/d = 2$.

For $\lambda/d = 1/4$, both the B- and E-schemes show the same distortion as for $\lambda/d = 2$. The C-scheme, however, now shows a monotonic decrease of frequency with increasing wavenumber. As a result, contrary to the exact solution, the phase speed at high wavenumbers for this scheme is much slower than that for low wavenumbers; furthermore, the direction of group velocity reverses resulting in the greatest distortion of the exact solution.

3. Numerical results

Based on the results in the previous section, proper dispersion of high frequency waves, i.e., inertia-gravity waves, occurs only for the C-scheme

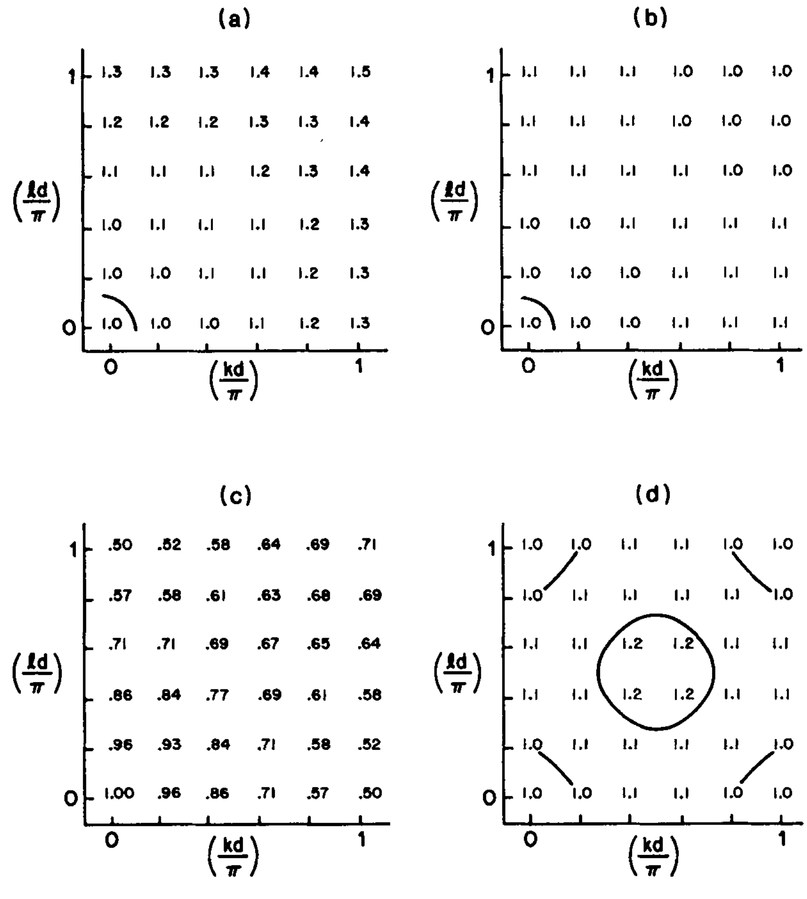

Fig. 3. Same as Fig. 2 except for $\lambda/d = 1/4$.

when $\lambda/d = 2$. For all other schemes and for $\lambda/d = 1/4$, distortion is always present in the high wavenumber region, precisely where dispersion should occur for proper simulation of the geostrophic adjustment process.

To examine the consequences of this distortion of wave frequency, a series of numerical initial-value problems was run using both space- and time-differencing schemes for the shallow water eqs. (1)–(3). Only the B- and C-schemes were used since they are the grid schemes currently used in OGCMs. In each experiment the fluid was initially at rest and was contained in a rectangular basin with zero normal velocity at the lateral boundaries. A point mass source and a point mass sink of 10 cm and -10 cm respectively, were prescribed at fixed locations 12-grid intervals apart at each time step; otherwise the initial height field was uniform. The shallow water equations were integrated using time steps of 450 seconds for one day, which is approximately the time required for geostrophic adjustment to occur. A cycle of an Euler-backward step and five subsequent integrations with the conventional leapfrog scheme was used for time integrations. The integrations were performed over a region of approximately 5500 km by 5500 km (25×25 grid intervals) for each scheme. The space and time increments satisfied the Courant–Friedrichs–Lewy condition.

Since, as shown in (3), the behavior of the height field delineates the divergent component of the flow associated with the dispersive inertia-gravity waves, only solutions for the height field are presented. These solutions at the 205th time step ($\sim$ the geostrophic adjustment time) are shown in Figs. 4 and 5 for the B- and C-schemes with equal spatial

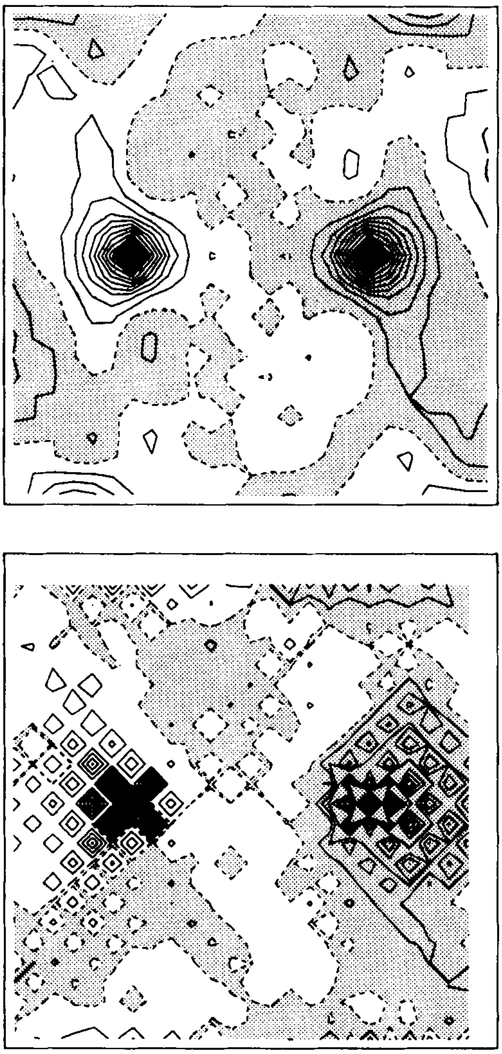

Fig. 4. The height field for $\lambda/d = 2$ for the C-scheme (top) and B-scheme (bottom) for equal grid intervals ($\Delta x = \Delta y = 220$ km). In all height fields which follow, the contour interval is 0.005 m with the dashed line at 0. Dotted regions denote negative height departures with respect to H. For both schemes the locations of the source and the sink regions are to the left and to the right, respectively, of the center point in each figure.

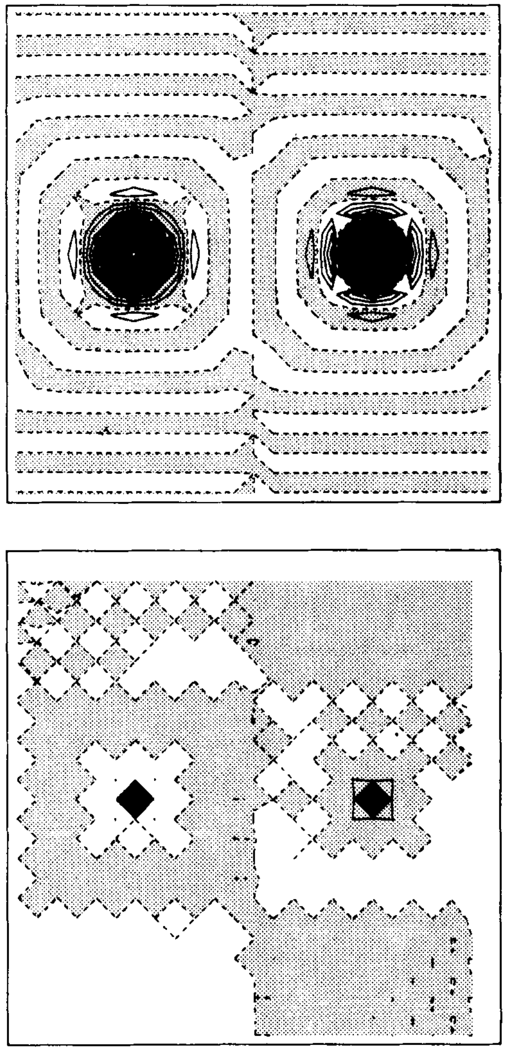

Fig. 5. Same as Fig. 4 except for $\lambda/d = \frac{1}{4}$.

grid intervals. Regardless of the (λ/d) ratio, the B-scheme has a checkerboard pattern of noise, shown by the alternation of positive and negative height areas in both figures. The C-scheme structure, however, is dependent on (λ/d): for the case $\lambda/d = 1/4$, a concentric two-grid interval noise is present as shown by the alternation of positive and negative height areas. Furthermore, close examination of time series for this scheme shows quasi-stationarity of the noise patterns.

The checkerboard noise pattern associated with the B-scheme is due to the averaging of the pressure gradient force, which renders the waves with this pattern as inertial oscillations rather than as dispersive inertia-gravity waves (Arakawa, 1972). The two-grid interval waves in the C-scheme, however, behave like gravity waves in a non-rotating fluid, due to the averaging of the Coriolis force. Because of the non-dispersive characteristic of gravity waves, these waves do not disperse the energy, resulting in the observed two-grid interval noise pattern.

To see whether or not the noise pattern is dependent on the grid size ratio, an asymmetric C-grid was examined (i.e., $\Delta x \neq \Delta y$) for the case $\lambda/d = 1/4$, which corresponds to the usual choice in coarse grid ocean models. The results are shown in Fig. 6 for the cases $\Delta x > \Delta y$ and $\Delta x < \Delta y$. When $\Delta x > \Delta y$, a predominantly north-south orientation of noise occurs, whereas when $\Delta x < \Delta y$ the orientation of the noise is more east-west. As shown in Fig. 5, both north-south and east-west orientations of noise are found when $\Delta x = \Delta y$. These results indicate that the choice of Δx and Δy influences the alignment of the noise pattern in the finite-difference grid.

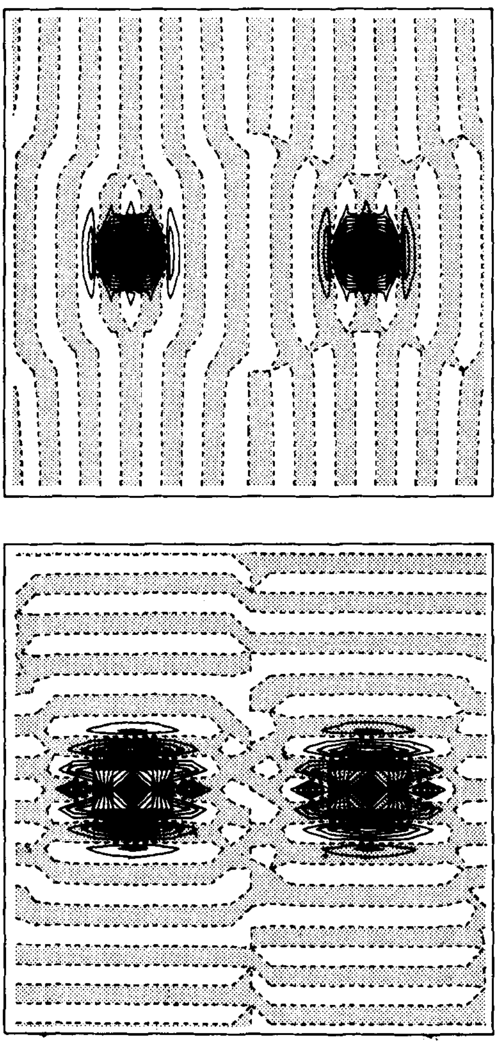

Fig. 6. The height field for unequal grid intervals Δx = 440 km, Δy =220 km, (top) and Δx = 220 km, Δy = 440 km (bottom) for $\lambda/d = 1/4$ for the C-scheme.

To further investigate this effect, the frequency equations were found for the B- and C-schemes, respectively, for the unequal grid intervals:

$$\left(\frac{\omega}{f}\right)^2 = 4\left(\frac{\lambda^2 \sin^2 \tfrac{1}{2}k\Delta x \cos^2 \tfrac{1}{2}l\Delta y}{(\Delta x)^2} + \frac{\lambda^2 \cos^2 \tfrac{1}{2}k\Delta x \sin^2 \tfrac{1}{2}l\Delta y}{(\Delta y)^2}\right) + 1 \qquad (9)$$

$$\left(\frac{\omega}{f}\right)^2 = 4\left(\frac{\lambda^2 \sin^2 \tfrac{1}{2}k\Delta x}{(\Delta x)^2} + \frac{\lambda^2 \sin^2 \tfrac{1}{2}l\Delta y}{(\Delta y)^2}\right) + \cos^2 \tfrac{1}{2}k\Delta x \cos^2 \tfrac{1}{2}l\Delta y \qquad (10)$$

Results for the case $\Delta x > \Delta y$ for both grids are shown in Fig. 7, which shows that the variation of (ω/k) is greater in the y-direction than in the x-direction. Thus, waves can propagate faster in the y-direction. Based on these results, when $\Delta x > \Delta y$ a north-south noise orientation should predominate over an orientation in the east-west direction. When $\Delta x < \Delta y$, the opposite noise alignment should occur.

Since we have found that the numerical noise for small (λ/d) ratios is present in both the B- and C-schemes for an inviscid flow, and because we must use small (λ/d) ratios in global ocean models, a successful technique to suppress the noise should be sought. In previous shallow water studies the use of a time alternating space-uncentered (TASU) differencing scheme has been shown by Arakawa (1972) to be effective for noise suppression in the B-scheme, whereas the use of a divergence-corrected scheme has been shown by Mesinger (1973) and Janjic (1974) to be effective for noise suppression in the E-scheme. However, since coarse grid OGCMs usually use a linear Laplacian-type dissipation with a large diffusion coefficient ($\sim 10^4$–10^5 m^2 s^{-1}), we have considered only the effect of this particular dissipation mechanism on suppressing the numerical noise found when small (λ/d) ratios are used. For both schemes second-order finite-differencing with no slip lateral boundary conditions were used. The results for λ/d = 1/4, corresponding to large grid sizes, and, accordingly, a large diffusion coefficient of 10^5 m^2 s^{-1}, are shown in Fig. 8. A comparison of Figs. 8 and 5

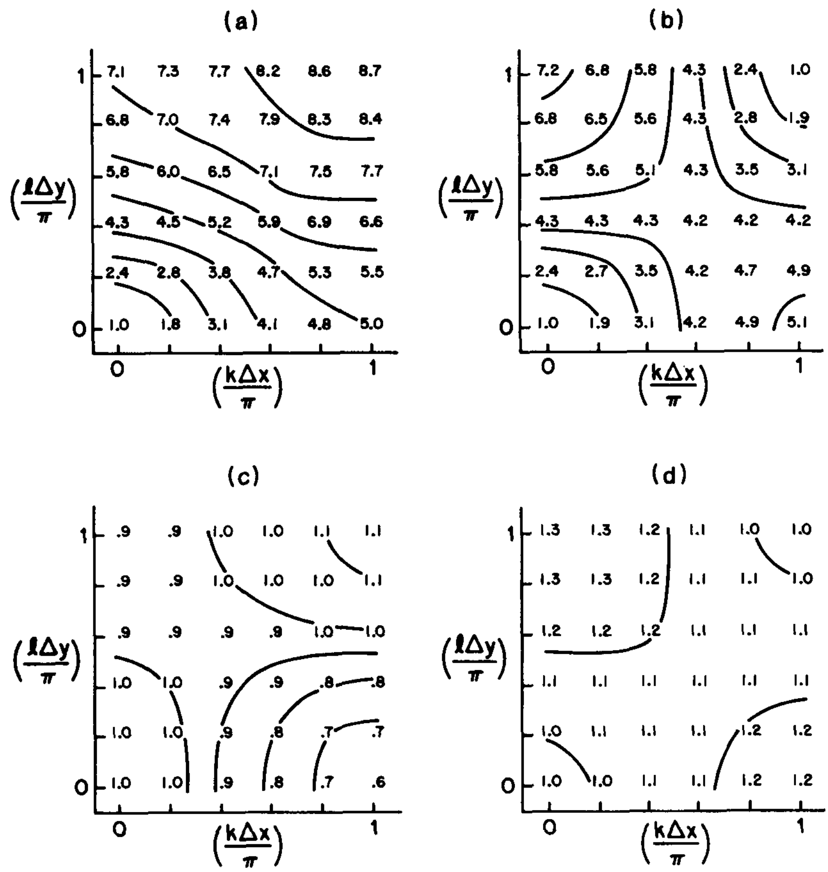

Fig. 7. Graphs of variation of (ω/f) as a function of dimensionless wavenumber for unequal grid intervals $\Delta x = 440$ km, $\Delta y = 220$ km. For $\lambda/d = 2$, (a) is for the C-scheme, (b) for the B-scheme; for $\lambda/d = 1/4$, (c) is for the C-scheme, (d) for the B-scheme.

for the C-scheme shows that regions of alternating positive and negative areas are still present, along with a change in the orientation of the two-grid interval noise near the southern and northern boundaries. A comparison of the same figures for the B-scheme shows that the checkerboard noise pattern in Fig. 5 has been replaced by smooth concentric height patterns around the source and sink regions in Fig. 8. Thus, the computational noise is successfully suppressed in the B-scheme when diffusion is included, but not in the C-scheme.

Use of a smaller diffusion coefficient of 10^4 m^2 s^{-1} for the B-scheme was also investigated; when compared with the height field in the case of no diffusion in Fig. 5 it was found that the fields were less noisy when this level of diffusion was included. However, some noise was still present, in contrast to the case of the large diffusion coefficient (Fig. 8). Hence, the use of a diffusion coefficient $\sim 10^4$ m^2 s^{-1} is sufficient for noise suppression in coarse B-schemes.

The question of why diffusion is more effective in one scheme than in another should be explored. Since Fig. 5 showed that the B- and C-schemes had different noise patterns, i.e., the B-scheme had checkerboard noise patterns while the C-scheme had either east-west or north-south noise patterns, the possibility that successful noise suppression might be related to the orientation of the noise was therefore investigated. Fig. 9 shows three hypothetical noise orientations, namely, east-west, north-south, and diagonal (or checkerboard). If the diffusion of some quantity ψ is taken as proportional to $\nabla^2\psi$ and is computed for each noise

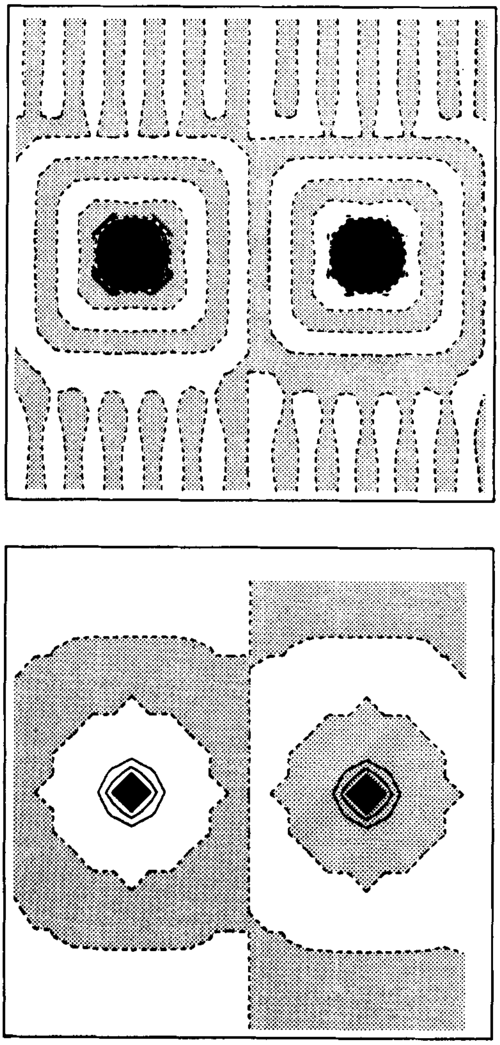

Fig. 8. The height field for equal ($\Delta x = \Delta y = 220$ km) grid intervals with diffusive dissipation for $\lambda/d = 1/4$ for the C-scheme (top) and B-scheme (bottom). The diffusion coefficient is 10^5 m^2 s^{-1}.

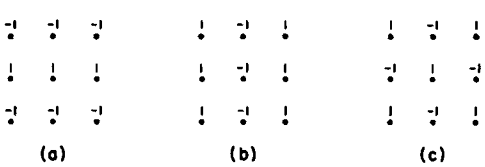

Fig. 9. Characteristic orientations of noise: (a) east-west oriented, (b) north-south oriented, and (c) diagonal (checkerboard pattern). The Laplacian of ψ for each noise pattern is $\nabla^2 \psi = -4/d^2$ for (a) and (b) and $-8/d^2$ for (c).

pattern, we find that the same diffusion coefficient is twice as effective in suppressing a checkerboard noise pattern (Fig. 9c) as it is for an east-west or north-south oriented noise pattern (Fig. 9a, 9b). However, the use of twice as large a diffusion coefficient (i.e., $\sim 2 \times 10^5$ m^2 s^{-1}) did not successfully suppress noise in the C-scheme. It is therefore suggested that other diffusive dissipation formulations such as biharmonic and nonlinear dissipations, and higher-order finite-differencing schemes, be explored for the C-scheme. However, since the main purpose of the present study is to examine the intrinsic properties of finite-differencing schemes for an inviscid rather than viscous fluid, we leave the systematic investigation of these techniques for future research.

4. Conclusions

The present study has shown that the general characteristics of numerical solutions of simple fluid flow depend critically upon the choice of model parameters as well as on grid schemes. Whereas the C-scheme is superior to the B-scheme for $(\lambda/d) > 2$, the B-scheme, if diffusive dissipation is included, appears to be a superior choice for $(\lambda/d) < 2$. Based on these results, and with the reservation that the present study is only appropriate for two-layer models (since the Rossby radius of deformation can be different for different baroclinic modes in multi-layer models), the C-scheme is a better choice than the B-scheme for fine-scale resolution (<50 km), as in ocean eddy-resolving models; the B-scheme with diffusion is recommended for coarse-grid models (>100 km) such as conventional OGCMs.

Although the present study provides a preliminary guide for the choice of grid schemes in ocean modeling, further research is needed before definitive conclusions regarding the best grid schemes for ocean modeling and for large-scale geophysical flows in general can be drawn. For example, further comparison could be made between time-dependent analytic solutions and numerical solutions. Attention could also be given to the evolution and behavior of the velocity field, since in the present study the velocity field in the B-scheme is nearly geostrophic regardless of (λ/d), whereas with the C-scheme the velocity field is highly divergent. Whether this is due to the grid schemes themselves or to the prescription of a singular mass source and sink in the height field is not known. To determine this, an analysis of the velocity field for different grid schemes with extensive forcing (i.e., wind stress) in place of the present singularities could be made. Nevertheless, our results indicate that, for coarse grid ocean models, the B-scheme with the use of diffusive dissipation can successfully suppress computational noise.

5. Acknowledgements

This research was supported by National Science Foundation Grant ATM-77-26406 and by National Aeronautics and Space Administration grant NSG-5353. We would like to thank Dr W. L. Gates for both his support and review of the manuscript, and Dr J.-W. Kim for his helpful discussions. We also extend appreciation to W. McKie for assistance in programming and to Diana Ramey for typing the manuscript.

REFERENCES

Arakawa, A. 1972. Design of the UCLA general circulation model. Tech. Rep. No. 7, Dept. Meteor., Univ. of Calif., Los Angeles, 116 pp.

Arakawa, A. and Lamb, V. R. 1977. Computational design of the basic dynamical processes of the UCLA general circulation model. In *Methods of Computational Physics*, vol. 17, Academic Press, New York, 173–265.

Blumen, W. 1972. Geostrophic adjustment. *Rev. Geophys. and Space Phys. 10*, 485–528.

Bryan, K. 1969. A numerical method for the study of the circulation of the world ocean. *J. Comput. Phys. 4*, 347–376.

Cahn, A. 1945. An investigation of the free oscillations of a simple current system. *J. Meteorol. 2*, 113–119.

Haney, R. L. 1974. A numerical study of the response of an idealized ocean to large-scale surface heat and momentum flux. *J. Phys. Oceanogr. 6*, 145–167.

Holland, W. R. and Lin, L. B. 1975. On the generation of mesoscale eddies and their contribution to the ocean general circulation. I. A preliminary numerical experiment. *J. Phys. Oceanogr. 5*, 643–657.

Janjic, Z. I. 1974. A stable centered difference scheme free of two-grid-interval noise. *Mon. Wea. Rev. 102*, 319–323.

Kim, J.-W. 1979. Design and preliminary performance of the OSU four-level oceanic general circulation model. Report No. 6, Climatic Research Institute, Oregon State University, Corvallis, 49 pp.

Mesinger, F. 1973. A method for construction of second-order accuracy difference schemes permitting no false two-grid interval wave in the height field. *Tellus 25*, 454–457.

Mesinger, F. and Arakawa, A. 1976. *Numerical methods in atmospheric models*. Garp. Publications Series No. 17. WMO/ICSU, 64 pp.

Mihaljan, J. M. 1963. An exact solution of the Rossby adjustment problem. *Tellus 15*, 150–154.

Pedlosky, J. 1979. *Geophysical Fluid Dynamics*. Springer-Verlag, New York, 624 pp.

Rossby, C.-G. 1938. On the mutual adjustment of pressure and velocity distributions in certain simple current systems, 2. *J. Mar. Res. 1*, 239–263.

Schoenstadt, A. L. 1978. A transfer function analysis of numerical schemes used to simulate geostrophic adjustment. Report NPS-53-79-001, Naval Postgraduate School, Monterey, Calif., 44 p..

Winninghoff, F. 1968. On the adjustment toward a geostrophic balance in a simple primitive equation model with application to the problem of initialization and objective analysis. Ph.D. dissertation, Univ. of Calif., Los Angeles, 161 pp.

О ВЫЧИСЛИТЕЛЬНОМ ШУМЕ КОНЕЧНО-РАЗНОСТНЫХ СХЕМ, ИСПОЛЬЗУЕМЫХ В МОДЕЛЯХ ОКЕАНА

Различные распределения переменных в точках горизонтальной сетки в модели циркуляции океана, основанной на уравнениях мелкой воды, исследуются с целью найти пути для выбора конечно-разностной схемы при моделировании океана. Для изучения типов вычислительного шума, присутствующего в каждой сетке, используется численная и аналитическая техника. Показано, что B-схема (в которой горизонтальная скорость вычисляется в центре, а поле высоты изобарической поверхности в каждом углу ирямоугольной сеткиф с диффузионной лиссипацией успешно подавляет вычислительный шум в модели океана с грубой сеткой (> 100 км). Для детального разрешения (< 50 км), как в мезомасштабных моделях океана, иоказано, что C-схема (в которой зональная скорость вычисляется в точках к востоку и западу от точек прямоугольной сетки, где вычисляется высота, а меридиональная скорость — к северу и югу от тех же точек) может быть свободна от шума для иервой моды как в двухслойной модели).